Microstratigraphic reconstruction of formation processes and paleoenvironments at the Early Pleistocene Cornelia-Uitzoek hominin site, Free State Province, South Africa

Michael Toffolo, James Brink, Francesco Berna

HAL Id: hal-02090808
https://hal.science/hal-02090808

Submitted on 22 Oct 2021

1 **Microstratigraphic reconstruction of formation processes and paleoenvironments at the Early**

2 **Pleistocene Cornelia-Uitzoek hominin site, Free State Province, South Africa**

3 Michael B. Toffolo[a,b,*], James S. Brink[a,c], Francesco Berna[d]

4 [a]Florisbad Quaternary Research Department, National Museum, 36 Aliwal Street, Bloemfontein

5 9300, South Africa.

6 [b]Institut de Recherche sur les Archéomatériaux-Centre de Recherche en Physique Appliquée à

7 l'Archéologie (IRAMAT-CRP2A), UMR 5060 CNRS, Université Bordeaux Montaigne, 8

8 Esplanade des Antilles, Pessac 33607, France.

9 [c]Centre for Environmental Management, University of the Free State, 205 Nelson Mandela Drive,

10 Bloemfontein 9300, South Africa.

11 [d]Department of Archaeology, Simon Fraser University, 8888 University Drive, Burnaby BC V5A

12 1S6, Canada.

13 *Corresponding author. Phone: +33 (0)5 57 12 46 81. Email address: michael.toffolo@u-bordeaux-

14 montaigne.fr

15 **Abstract**

16 The Cornelia-Uitzoek fossil site has produced a large collection of bones, Acheulean artifacts and a

17 *Homo* sp. tooth dated to ~1 million years ago. The faunal assemblage defines the Cornelian Land

18 Mammal Age and is characterized by a number of extinct species of large mammals that reflect an

19 open grassland environment. Bones were accumulated by hyenas, whereas artifacts appear to be

20 chance inclusions, although they suggest human presence in the immediate surroundings. Previous

21 studies established the absolute chronology of the site and a broad stratigraphic sequence. However,

22 the sedimentary units identified in the field were not linked to specific formation processes, thus

23 limiting the understanding of the depositional history of the site and its potential in reconstructing

24 Pleistocene environments. Using a microgeoarchaeological approach based on infrared

25 spectroscopy and micromorphology of sediments, we were able to determine the formation and

26 post-depositional processes of the entire stratigraphic sequence, and to show that the site is

27 characterized by alluvial sediments accumulated under different river flow regimes. Our results

28 provide context to the faunal and lithic assemblages and are in agreement with existing

29 paleoenvironmental data for the site.

30 **Keywords:** paleoenvironment; micromorphology; FTIR; Cornelian; Acheulean; formation

31 processes; South Africa

1 Introduction

Early Pleistocene open-air archaeological and fossil sites are rather rare occurrences in the central interior of South Africa, as they are confined to preserved "pockets" of sediments bearing artifacts and bones deposited in the shallow valleys of meandering rivers, such as the Vaal and its tributaries (e.g. Mason, 1961; Helgren, 1978; Li et al., 2017; Kuman and Gibbon, 2018). Considered their paucity, these sites are an exceptionally important source of information about hominin adaptation to open landscapes and changing environments, especially in a region located outside the Malmani dolomitic karst landscape that is home to the Cradle of Humankind, which produced a large number of fossils including hominin remains (Eriksson and Altermann, 1998; Kuman, 2016). Therefore, the characterization of paleoenvironments at these alluvial sites using sediments and bones as a proxy holds considerable value for our understanding of the evolution of early hominins in southern Africa.

One of these notable localities in the interior is Cornelia-Uitzoek, a Pleistocene fossil-bearing site near the town of Cornelia, in the Highveld plateau of the northeastern Free State Province of South Africa (henceforth Free State), at 1540 m a.s.l. (Figure 1). The site is the type locality of the Cornelian Land Mammal Age (LMA), a period between ~1.1 and 0.6 Ma characterized by a number of extinct species of large mammals that follows the Makapanian and precedes the Florisian LMAs (Cooke, 1974; Hendey, 1974; Lacruz et al., 2002; Brink, 2004; Brink et al., 2012). In addition, Cornelia-Uitzoek has produced a substantial assemblage of Acheulean artifacts and a *Homo* sp. tooth dated to ~1 Ma (Clark, 1974; Brink et al., 2012).

The most prominent faunal occurrence found at the site is a large bone bed located at the bottom of the sequence, which was dated to ~1 Ma using paleomagnetism (Brink et al., 2012). Bones make up the typical Cornelian assemblage dominated by open-grassland and water-dependent species and were accumulated by hyenas in a burrow, as suggested by the presence of coprolites and gnawing marks. The same locality yielded the largest concentration of Acheulean artifacts at the site, including handaxes and cleavers. At present there is no explicit link between bones and artifacts, which are interpreted as chance inclusions in the bone bed from an ancient land surface, based on their random occurrence throughout the deposit and on the absence of cutmarks on bones (Brink, 2004). It should be noted that the presence of all stages of the operational chain except for cores may indicate local finishing and use of bifaces (Brink et al., 2012).

The study of Brink et al. (2012) established a general stratigraphic sequence of the site by differentiating sediment types at the macroscopic scale. However, sedimentary features were not linked to specific formation processes, and as a result the depositional history of the site is not well

understood, especially in relation to faunal assemblages. Therefore, the present study is aimed at addressing outstanding questions regarding site formation processes, including how the latter can provide insights into changing paleoenvironments during the Early Pleistocene. To achieve this goal, we employed a microgeoarchaeological approach based on Fourier transform infrared spectroscopy (FTIR) and micromorphology of sediments, which address different aspects of the microscopic record (e.g. Goldberg and Berna, 2010; Weiner, 2010; Karkanas and Goldberg, 2019). More specifically, FTIR was used to differentiate clay minerals and determine the preservation state of bones, whereas micromorphology allowed the study of sediments at the microscopic scale and within their original depositional context. By doing so, we were able to identify microscopic sedimentary structures and components related to different regimes of alluvial deposition and post-depositional alteration, which are in agreement with other paleoenvironmental proxies, such as faunal assemblages and stable isotopes analysis of tooth enamel. In addition, our results support the interpretation of the bone bed formation proposed by Brink (2004), according to which hyenas burrowed an existing paleo-donga, and provide context to the local landscape in which early hominins lived.

2 Materials and methods

2.1 Site settings and sampling strategy

The Cornelia-Uitzoek occurrence was discovered and excavated in the 1920s by E. C. N. van Hoepen, who first described the stratigraphic sequence and faunal collection (van Hoepen, 1930, 1932b, a, 1947). Another excavation season led by A. C. Hoffman took place in 1953 (Clark, 1974), whereas K. W. Butzer later described the sedimentary context (Butzer, 1974). Surface collection of fossils was resumed in the early 1990s by J. S. Brink (Bender and Brink, 1992), who started a new excavation program in 1998 (Brink and Rossouw, 2000).

The latest investigations uncovered a large amount of faunal and lithic evidence, and determined its chronology and geomorphological context (Brink et al., 2012). The site is located within a pocket of alluvial clay and gravel deposits carved into the local Permian shale bedrock of the Ecca Group (Karoo Supergroup), a mudstone made of clay minerals and fine-grained quartz. Shale has been intruded in places by Jurassic dolerite, a mafic subvolcanic rock similar to basalt (see Toffolo et al., 2017 for a detailed mineralogical description). The alluvial sequence has been incised by the Schoonspruit River, a left-bank tributary of the Vaal River that flows in a northerly direction, about 50 m west of the site (Tooth et al., 2004). Geological and climatic constraints and the limited bedload of the Schoonspruit in recent times favored bank erosion, which determined the formation of deep erosional gullies, locally termed "dongas" (Figure 2 and Figures S1-S4). These

98   features exposed clusters of fossils and artifacts at different elevations within the stratigraphic

99   sequence.

100   In this study we followed the stratigraphic sequence and sedimentary units established by

101   Brink et al. (2012), which is summarized in Table 1. From bottom to top, the sequence features

102   Ecca shale, Banded Gravel Bed (BGB; Figure 3), Mottled Yellow Clay (MYC; Figure 4),

103   Laminated Orange Clay (LOC; Figure 5-6), Orange Coarse Gravel (OCG; Figure 7), Dark Grey

104   Clay (DGC) and Black Turf Soil (BTS; Figure 8). The bone bed appears as a linear and horizontal

105   intrusive feature (such as a burrow), about 2.5 m long, with limited vertical displacement of bones

106   (50 cm) and a poorly consolidated sedimentary matrix compared to the surrounding MYC (Figure

107   4) (Brink, 2004: Figure 4). These features led Brink (2004) to propose that hyenas reused and

108   burrowed an existing paleo-donga or similar erosional feature to make their lair.

109   In order to determine the formation processes that led to the accumulation of the deposits

110   and to reconstruct paleoenvironments based on the sequence of different sedimentary environments,

111   we opted for a microgeoarchaeological approach geared towards the identification of mineral

112   components and diagnostic sedimentary structures (Goldberg and Berna, 2010; Karkanas and

113   Goldberg, 2019). In particular, we used FTIR spectroscopy to characterize clay minerals and bones,

114   and micromorphology of sediments to observe microstratigraphy and all the features and

115   components that are not visible to the naked eye but contain valuable embedded information

116   regarding depositional processes.

117   Sediment and bone samples were collected from freshly exposed sections of the bone bed

118   (MYC unit) and different locales within the dongas in order to study the full stratigraphic sequence,

119   which is not entirely represented in one single section (Figure 3-8). Depositional units were

120   sampled at different locales and multiple bulk sediment samples were collected at random intervals

121   to address lateral variability. However, at the macroscopic level sedimentary units appeared

122   homogeneous over tens of meters and thousands of square meters in surface area. The DGC was not

123   recognized as a separate sedimentary unit in the field and thus was not sampled. Bones were

124   randomly selected from the bone bed collection curated at the Florisbad Research Station of the

125   National Museum to study their degree of diagenesis. Samples were immediately analyzed at an on-

126   site laboratory that included an infrared spectrometer and a petrographic microscope (Weiner,

127   2010). Preliminary information on mineral components and particle size was obtained with smear

128   slides. A few milligrams of bulk sediment sample were mounted onto a glass slide using Entellan

129   New (Merck) and analyzed at the on-site laboratory using a Nikon Optiphot petrographic

130   microscope at different magnifications (20x, 50x, 100x, 200x, 400x).

2.2 Fourier transform infrared spectroscopy (FTIR)

Bulk sediment samples were collected using a stainless-steel spatula, placed in 40 ml plastic vials marked with progressive sample numbers, and their composition was determined at the site using FTIR spectroscopy. After return to the home laboratory at the Florisbad Research Station, bones were analyzed as well to determine their degree of preservation. A few milligrams of each sediment (*n*=57) and bone (*n*=15) sample were homogenized and powdered in an agate mortar and pestle. About 0.1 mg were left in the mortar, mixed with approximately 0.5 mg of KBr (FTIR grade, Sigma-Aldrich) and pressed into a 7-mm pellet using a hand press (PIKE Technologies). Infrared spectra were obtained at 4 cm^{-1} resolution in 32 scans within the 4000-400 cm^{-1} spectral range using a Thermo Fisher Scientific Nicolet ™ iS5 spectrometer. Phase identification was performed using OMNIC v. 9, standard literature (Farmer, 1974; van der Marel and Beutelspacher, 1976), and the reference collection of FTIR spectra of standard materials provided by the Kimmel Center for Archaeological Science, Weizmann Institute of Science (http://www.weizmann.ac.il/kimmel-arch/infrared-spectra-library).

2.3 Micromorphology of sediments

Micromorphology was used to study sediments within their original depositional context, in order to determine their formation and post-depositional processes. Boundaries between sedimentary units were selected to highlight changes in depositional environments. In addition, samples from the middle portion of the MYC unit and bone bed were collected to differentiate their contents. Intact blocks of sediment (*n*=11) were carved from sections, air-dried for several weeks and finally oven-dried at 40°C for three days. Samples were then embedded in a mixture of polyester resin (NCS General Purpose Polyester) and acetone (ratio 7:3), with the addition of 1.5 ml catalyst per liter of mixture. Hardened blocks were sliced with a rock saw to obtain 55x75 mm chips, which were shipped to Arizona Quality Thin Sections (Tucson, Arizona, USA) for thin section preparation. Two additional samples were prepared at the thin section laboratory of the University of Bordeaux (France). All the thin sections were polished to a thickness of 30 µm. Micromorphological analyses were carried out using Olympus BX41 and Leica DM2500 P petrographic microscopes at different magnifications (20x, 25x, 40x, 50x, 100x, 200x, 400x). Descriptions and interpretations are based on conventional criteria developed in the specialized literature (Courty et al., 1989; Delvigne, 1998; Stoops, 2003; Flügel, 2004; Goldberg and Macphail, 2006; Stoops et al., 2010; Macphail and Goldberg, 2017). We use here the concept of "microfacies" (MFT) as described by E. Flügel, i.e. *"the total of all sedimentological and paleontological data which can be described and classified from thin sections* […]" (Flügel, 2004: 1). This term defines discrete assemblages of sediment types

164   based on the information retrieved from the analysis of thin sections. Considered that some

165   depositional units occur repeatedly throughout the stratigraphic sequence (e.g. MYC and LOC) and

166   that multiple thin sections were obtained from these units, the use of MFTs allows rapid reporting

167   of results. This approach to the study of thin sections includes the basic interpretive level of each

168   MFT (e.g. Goldberg and Aldeias, 2018).

169   **3 Results**

170   The chemical phases identified with FTIR spectroscopy are displayed in Figure 8. Sedimentary

171   components and structures observed in thin section are shown in Figure 9 and Figure 10; MFTs are

172   listed in Table 2. Below follows a description of the stratigraphic sequence from bottom to top,

173   based on the framework established by Brink et al. (2012). Micromorphological terminology by

174   Stoops (2003) is noted in *italics* between brackets next to the explanation of the relative feature at

175   its first appearance.

176   *3.1 Bedrock and Banded Gravel Bed*

177   The sedimentary sequence rests on top of Ecca shale. An unconformity separates bedrock from the

178   BGB (Figure 3), a layer of gravel characterized by normal graded bedding and dated to the

179   Matuyama reversal (>1.07 Ma). The coarse components (mainly cobbles to very fine pebbles with a

180   few boulders at the base) are mostly fragments of Ecca shale and Jurassic dolerite and they are

181   supported by a clayey matrix towards the top. Cross bedding is visible in places.

182   *3.2 Mottled Yellow Clay and Laminated Orange Clay*

183   The next unit in the sequence is the MYC (Figure 4), a layer of massive pale-yellow to pale-green

184   clay (depending on moisture), dated to the Jaramillo subchron (1.07-0.99 Ma). This deposit includes

185   the hyena bone bed that yielded a rich assemblage of Cornelian-age fossils, a human tooth, and

186   Acheulean artifacts (Brink, 2004). The sedimentary matrix of this layer comprises a mixture of clay

187   minerals of the smectite (dominant) and kaolinite (minor) groups, as indicated by the absorptions at

188   3690, 3620, 1090, 1032 and 525 cm^{-1}, and a minor amount of quartz (absorptions at 797, 779, 694

189   and 470 cm^{-1}) and feldspars (absorption at 646 cm^{-1}). Yellow mottles exhibit stronger absorptions of

190   kaolinite clays at 3697, 3620, 1009, 911, 791, 750, 670 and 536 cm^{-1} (Figure 9). Black clay nodules

191   rich in manganese oxides occur in places (broad absorption at 3405 cm^{-1}). Bones are characterized

192   by the occurrence of fluoridated carbonate hydroxyapatite on the outer surface of cortical tissue

193   (absorption at 604 cm^{-1} higher than the absorption at 567 cm^{-1}; Figure 9) (Geiger and Weiner,

194   1993).

195   Observed in thin section, the MYC shows the characteristic features of the "clay" MFT
196   (Table 2), which exhibits a dominant fraction of silt-sized grains of quartz and feldspar embedded
197   in a pale-green clay (*porphyric c/f related distribution*). Coarser sand-sized grains occur frequently,
198   thus making the coarse fraction poorly to moderately sorted. Porosity is represented by thin,
199   elongated voids that separate angular blocks of sediment (*angular blocky microstructure* with
200   *planes*), with a few cylindrical, elongated voids (*channels*). Below the level of the bone bed, the
201   fabric of the coarse fraction appears to be oriented horizontally in places due to bedding;
202   fragmented, horizontal silty-clay crusts showing normal graded bedding occur as well (Figure 10a-
203   b). No bedding was observed within the bone bed fill, and a substantial proportion of rounded, very
204   fine pebbles (2-4 mm) of shale make up the coarse fraction together with poorly sorted quartz
205   sand/silt (Figure 10c). The poor degree of compaction of shale pellets determines the occurrence of
206   voids resulting from loose packing (*simple packing voids*) and in general of greater porosity
207   compared to lower levels. Throughout the entire layer, the fine fraction is characterized by domains
208   of clay minerals oriented in small patches, along random straight lines, or around grains and pores,
209   as evidenced by their birefringence fabric (*stipple speckled, striated, granostriated and porostriated*
210   *b-fabric*, respectively; Figure 10d). Post-depositional processes (*pedofeatures*) are represented
211   mainly by the translocation of clays through groundwater movement. Two distinct events were
212   observed: dense accumulations of clay in pores (*intercalations*) and void coatings composed of
213   dark-green clay; laminated void coatings and dense void infillings of yellow clay, often juxtaposed
214   to the dark-green clay features (Figure 10e-f). In addition, different types of Fe-Mn oxide aggregate
215   nodules are superimposed on the fine fraction, shale fragments and clay coatings/infillings (Figure
216   10g). Reddish Fe-Mn oxide halos around pores (*hypocoatings* and *quasicoatings*) occur as well
217   (Figure 10h).

218   A sharp erosive boundary separates the MYC from the LOC (Figure 5-6), a layer composed
219   of alternated beds of clay and fine gravel and dated to the Matuyama reversal (0.99-0.78 Ma). Clay
220   beds exhibit the same FTIR spectra as the MYC, with black patches of Fe-Mn oxides and yellow
221   mottles richer in kaolinite minerals, whereas gravel is composed of rounded fine pebbles of local
222   Ecca shale. Bones exhibit absorptions of fluoridated carbonate hydroxyapatite.

223   Clay beds show the microscopic characteristics of the "clay" MFT (Table 2). In addition to
224   the features observed in the MYC, the LOC clay beds exhibit cm-deep bands of diffuse Fe oxide
225   halos (*impregnations*) (Figure 11a), close to the boundary with the overlying layer. These bands are
226   superimposed on the fine fabric (*groundmass*) and represent ancient surface zones of enhanced Fe
227   oxidation, favored by a concentration of plant material and microorganisms in a fluctuating water
228   table, possibly in relation to river floods (Courty et al., 1989; Lindbo et al., 2010). A similar process

229   occurred in the case of dense void infillings composed of silt embedded in red clay (Figure 11b).

230   These pedofeatures are related to the presence of root casts of woody and/or herbaceous plants, a

231   common occurrence at the site (Figure 12). These vertical channels are pseudomorphs of roots

232   derived from ancient surfaces and were observed throughout the entire sedimentary sequence,

233   except for topsoil. The decay of plant material due to microorganism activity favors the

234   mobilization of Fe and its subsequent precipitation due to exposure to air in the channel left by the

235   root (Lindbo et al., 2010). This is later infilled by coarse sediment from the overlying layer.

236   Furthermore, clay beds are characterized by a greater proportion of Fe-Mn oxide aggregate nodules.

237   Gravel beds show the characteristic features of the "fine gravel" MFT (Table 2). Coarse

238   fraction is composed of shale pebbles (very fine to medium) linked by clay bridges that often coat

239   grains (*chitonic* to *concave gefuric c/f related distribution*), whereas fine fraction is rarely present

240   (Figure 11c). Pores derive from the spatial arrangement between pebbles and from their degree of

241   compaction (*weakly separated granular microstructure* to *vughy microstructure* with *compound*

242   *packing voids*, *regular vughs* and *star-shaped vughs*). Similar to previous sedimentary units, the

243   LOC exhibits juxtaposed dark-green and yellow clay coatings with superimposed Fe-Mn aggregate

244   nodules (Figure 11d).

245   *3.3 Orange Coarse Gravel and Black Turf Soil*

246   Another sharp, wavy and erosive boundary, which corresponds to the beginning of the Brunhes

247   chron (<0.78 Ma), marks the transition between the LOC and the OCG (Figure 7). Clasts are

248   medium to very coarse pebbles and show different fabric depending on the location within the

249   layer. Cross-bedding and imbrication are visible in places, especially in the lower portion of the

250   unit.

251   The chemical composition of the fine fraction is comparable with the MYC and LOC,

252   showing a mixture of kaolinite (dominant) and smectite clay minerals (Figure 9). Bones were not

253   found in this sedimentary unit. A number of cm-size nodules coated with a black film exhibit

254   absorption bands of kaolinite and Fe-Mn oxides. These components are concentrated at the

255   transition with the overlying topsoil and can be observed today at the top of the donga as a lag

256   product of the erosion of finer topsoil material (Figure 13).

257   The microscopic features of the OCG can be grouped under the "coarse gravel" MFT (Table

258   2), which presents similarities with the "clay" MFT. More specifically, the poorly sorted coarse

259   fraction is embedded in yellow clay (*porphyric c/f related distribution*) and is characterized by

260   planes (*angular blocky microstructure*); the fine fraction exhibits prominent striated, porostriated

and granostriated b-fabrics. However, there are also notable differences, namely the greater proportion of coarse particles, the occurrence of considerable amounts of dolerite pebbles (Figure 11e) and Fe-Mn oxide typic nodules, and the absence of intrusive pedofeatures, such as clay coatings. Oxide nodules are mainly round and exhibit sharp boundaries, implying that they formed elsewhere within the OCG before reaching their final location (*disorthic nodules*). Other nodules instead clearly formed in situ (*orthic nodules*), as suggested by their irregular boundary or concentric appearance (Figure 11f-g).

The OCG grades into the BTS (Figure 8), a soil profile characterized by an orthic A horizon (Soil Classification Working Group, 1991). As stated, the transition boundary exhibits a large number of 0.5-1 cm round pellets composed of Fe-Mn oxides. In places, especially at the top of dongas and close to the erosion line, the BTS plant cover has disappeared, thus exposing soil horizon to rain, erosion, and oxidation of organic compounds. The latter favored a change in color from brown to dark grey, hence the thin Dark Grey Clay (DGC) layer reported by Brink et al. (2012) as patches in between the OCG and BTS (Figure 14). In addition, the DGC layer is characterized by large accumulations of Fe-Mn oxide pellets left behind as lag deposit after the erosion of fine material. Therefore, the DGC appears to be a weathering product of the BTS and thus its description coincides with the latter.

Looking at FTIR spectra, the BTS sediments are composed of a mixture of kaolinite (dominant) and smectite clay minerals, quartz and feldspars. Compared to the MYC and LOC, they contain a larger proportion of kaolinite minerals. The microscopic features of this sedimentary unit are ascribed to the "topsoil" MFT (Table 2) and comprise a poorly sorted coarse fraction (quartz silt and sand) embedded in a dark-brown clay with undifferentiated b-fabric and large amounts of amorphous organic matter. Plant fibers occur as well and are part of the current vegetal cover. Porosity is almost absent and confined to a few channels created by plant roots in an otherwise massive microstructure. The latter is disrupted by extensive areas of intense bioturbation, as indicated by the presence of *Oribatida* mites excrements (Figure 11h) (Kooistra and Pulleman, 2010). Besides faunal activity, pedofeatures include typic orthic and disorthic nodules of Fe-Mn oxides, especially close to the boundary with OCG.

4 Discussion

The results of FTIR and micromorphological analyses presented herein allow the interpretation of the stratigraphic sequence in relation to archaeological, faunal, geologic and environmental evidence previously published for the site and the region.

293 *4.1 Formation and post-depositional processes*

294 Starting from the bottom, it appears that the unconformity between bedrock and BGB may account

295 for multiple cycles of sedimentation and erosion that took place between the Permian and Early

296 Pleistocene, a common feature in southern African sedimentary contexts, including the Free State

297 (e.g. Loock and Grobler, 1988; Toffolo et al., 2017). Based on the large clast size (up to boulders),

298 the BGB is a point bar or channel deposit accumulated under high-energy water conditions

299 consistent with a braided river system, perhaps the paleo-Schoonspruit, whose catchment basin

300 drained an area characterized by local Karoo-aged lithology.

301   Further up in the sequence, the localized horizontal fabric of the coarse fraction and the

302 presence of clay crusts lend support to the interpretation of the MYC as an overbank deposit in a

303 meandering paleo-Schoonspruit, characterized by low-energy water; in particular, clay crusts

304 represent remnants of ancient depositional surfaces (Courty et al., 1989; Vingiani et al., 2018).

305 Instead, the bone bed fill shows no layering and a greater proportion of pores (low compaction) and

306 coarse components, including rounded, very fine pebbles of shale and poorly sorted quartz. These

307 features are consistent with a chaotic accumulation of sediment as infill of a "pocket" within the

308 MYC, which might be the result of hyena burrowing and bone concentration, and colluvium

309 deposition as observed in present-day donga channels (Figure 15). Micromorphological

310 observations thus seem to support the interpretation advanced by Brink (2004) and Brink et al.

311 (2012) regarding the location of the hyena den within a paleo-donga or channel created by localized

312 erosion in the vicinity of the river.

313   Bones appear to be well preserved, and this is confirmed by the occurrence of fluoridated

314 carbonate hydroxyapatite. This mineral is known to form in extremely old fossils (e.g. Piga et al.,

315 2011) and in more recent bones exposed to fluoride-rich groundwater (e.g. Toffolo et al., 2015) due

316 to the replacement of OH^- ions with F^- ions in more symmetrical locations within the crystal lattice

317 of carbonate hydroxyapatite. As a result, bone mineral becomes more resistant to chemical

318 weathering (Newesely, 1989; LeGeros, 1991). Based on their good state of preservation from both

319 the morphological and chemical point of view, bones must have been exposed on the surface only

320 briefly, and the bone bed buried rather quickly by overlying sediments.

321   In addition, several post-depositional processes considerably affected the MYC. First, the

322 striated b-fabric and angular blocky microstructure are typical of shrink/swell processes in smectites

323 (Courty et al., 1989), which were identified with FTIR, and are consistent with a pronounced vertic

324 behavior of sediments (Toffolo and Berna, 2008; Kovda and Mermut, 2010). These processes likely

325 contributed to the slight slumping and fragmentation of some bone specimens observed by Brink

10

326 (2004). Second, pores are often coated/filled with dark-green clay and yellow clay. The former is

327 the result of fine illuviation from a vegetated topsoil, now lost, that developed on the MYC layer,

328 whereas the latter may be ascribed to several episodes of fine illuviation (based on the laminated

329 appearance of the coatings) from overlying layers (Courty et al., 1989), e.g. the OCG; according to

330 FTIR, yellow clay mottles include a larger proportion of kaolinite minerals compared to the general

331 sedimentary matrix, and that is the main component of clay minerals in the OCG. Third, the

332 presence of Fe-Mn redoximorphic features in the form of coatings and nodules juxtaposed or

333 superimposed on coarse and fine components points to periodic waterlogging of sediments (Courty

334 et al., 1989). Fe and Mn ions are mobilized under waterlogged conditions and subsequently oxidize

335 upon drying, creating aggregate nodules and hypo- and quasi-coatings of pores (Lindbo et al.,

336 2010). The antiquity of these pedofeatures is demonstrated by the occurrence of yellow clay

337 coatings in voids characterized by Fe-Mn oxide hypo-coatings (Figure 10h). In addition, the fact

338 that bones exhibit Mn staining and patches of fluoridated carbonate hydroxyapatite indicates they

339 were exposed for prolonged periods to groundwater rich in both elements.

340   The MYC and LOC appear to be the product of similar formation and post-depositional

341 processes. The thick layer of MYC was deposited as overbank during floods and provided the

342 surface where hyenas dug their lair and accumulated carcasses. The same land surface was likely

343 characterized by human presence and possibly sporadic occupation; the occurrence of Acheulean

344 handaxes and cleavers together with flakes and blanks suggests that artifacts were produced close to

345 the site (Brink et al., 2012). Their inclusion in the bone bed fill could be due to deliberate discard,

346 or it might be the result of the burrowing activity of hyenas and later colluvium in the paleo-donga

347 channel. In the absence of clear occupation surfaces, the latter hypothesis seems the most likely

348 based on micromorphological data. However, this does not rule out the possibility that humans

349 roamed the site (as indicated by the tooth). The erosive contact with the overlying LOC, which

350 corresponds to a stripped land surface from which the dark-green clay translocated downwards into

351 voids, marks a change in the depositional pattern, with clay beds similar to the MYC that alternate

352 with fine gravel beds accumulated under conditions of slightly higher-energy water. As observed in

353 the field, where multiple bone scatters were recorded at different levels within the LOC, each of the

354 clay and fine gravel beds provided temporary land surfaces that functioned as accumulation sites for

355 bones and artifacts, although not in the same proportions as in the hyena bone bed. Given the small

356 size of these bone assemblages and the cyclic sedimentary pattern, it appears that hyenas were not

357 the primary depositional agent of bones in the LOC. The presence of Fe oxide bands and root casts

358 seems to support the occurrence of stable vegetated surfaces at different stages in the formation of

359 the sedimentary unit, which would have encouraged human settlement of the area.

The large amount of pebble-sized clasts and the presence of cross-bedding and imbrication indicate that the OCG was deposited by high-energy water in a point bar or straight channel of a meandering river system (Courty et al., 1989). After deposition, this sedimentary unit underwent shrink/swell processes, represented by the prominent striated b-fabric. In addition, a large portion of the yellow clay that makes up the fine fraction translocated into the LOC and MYC through eluviation processes, thus creating the yellow clay coatings and infillings observed in lower units. In fact, the OCG is today the least visible sedimentary unit at the donga, due to its lower resistance to weathering. Its dissolution promoted the accumulation of a thin layer of shale clasts and Fe-Mn oxide nodules, which were left behind as lag deposit.

One last episode of alluvial deposition in conditions of low-energy water promoted the formation of the BTS. In addition, the presence of medium and coarse sand rounded grains of quartz points to an eolian component of the coarse fraction. This is a common characteristic at terminal Pleistocene-Holocene sites in the Free State (e.g. Lyons et al., 2014; Toffolo et al., 2017). This sedimentary unit lacks secure chronological pegs but considering the occurrence of sporadic Middle Stone Age artifacts and the almost completely reworked nature of the sediments, it seems that the age of this layer may well exceed 50 ka.

4.2 Paleoenvironments

Given the scarcity of paleo-climatic data for the Free State before 500 ka (e.g. deMenocal, 2004; Scott and Neumann, 2018), it is difficult to draw interpretations in that sense based solely on the sedimentary context. In addition, river flow in this region has been shown to be primarily affected by the erosion and retreat of dolerite knickpoints, which determine the slope and degree of sinuosity of riverbeds, rather than climate. The retreat of knickpoints ultimately depends on base level fall rates of the Vaal, which in the Plio-Pleistocene were governed by a complex mix of tectonic uplift and climate change at the regional level (Tooth et al., 2004 and references therein). However, recent paleoenvironmental data for the Limpopo River catchment basin, located to the immediate northeast of the Free State, show an increase in aridity after 1 Ma (Caley et al., 2018). Therefore, assuming wetter conditions before this threshold, which may have implied an increased flow regime of the Vaal and other rivers in the region and thus faster riverbed incision, it would seem that the BGB and the erosional hiatus with the overlying MYC were formed as a result of knickpoint retreat and larger water supply at the source. More detailed sedimentary and climatic data for this period in the northeastern Free State is nevertheless required in order to support this suggestion.

The occurrence in the bone bed of ungulates and water-dependent species, such as *Hippopotamus gorgops* (giant hippo) and *Syncerus antiquus* (giant long-horned buffalo) (Brink,

393 2004; Brink et al., 2012), together with the low-energy water environment characteristic of

394 meandering rivers, suggest that the MYC represents a grassland landscape characterized by surface

395 waters (i.e. oxbows, backwaters and swamps), similar to what is observed today in the upper reach

396 of the Klip River in the Memel Seekoeivlei Nature Reserve, located about 70 km east of Cornelia.

397 There, in areas characterized by soft sandstone bedrock away from dolerite outcrops and

398 knickpoints, the river meanders within a large valley, creating oxbows and backswamps during

399 summer rains (Tooth et al., 2002). This kind of environment probably developed also in the broad

400 shale valley of the paleo-Schoonspruit around Cornelia-Uitzoek, thus attracting herbivores and with

401 them carnivores and humans. Therefore, sedimentary and faunal evidence show that during the

402 Early Pleistocene the central interior of South Africa offered a lush habitat favorable to human

403 settlement, besides the well-known Malmani dolomitic karst. A later parallel in terms of grassland

404 paleoenvironment with plenty of water is represented by Florisbad, in the mid-western Free State

405 (e.g. Brink, 1987, 1988; Kuman et al., 1999; Brink and Henderson, 2001; Toffolo et al., 2017).

406   The formation of pedofeatures caused by shrink-swell episodes during the Pleistocene (i.e.

407 dark-green clay coatings juxtaposed to subsequent yellow clay coatings originated from younger

408 units), lends support to the hypothesis of the existence of a summer rainfall regime already at that

409 time. Prolonged periods of drought during winter months and rainfall concentrated in summer may

410 account for the presence of shrink/swell features. The possible existence of a paleo-donga, as

411 suggested by thin sections, would also be a product of seasonal rains. This scenario seems in

412 agreement with faunal data. Several individuals from the bone bed exhibit enamel $\delta^{13}C$ values

413 >0‰, which are characteristic of a diet based on C_4 grasses, and diagnostic phytoliths from these

414 plants were recovered from the same context (Codron et al., 2008). Plants that produce energy

415 through C_4 processes typically grow in environments where groundwater is scarcely available due

416 to high evapotranspiration, and this is a common trait of the Highveld grasslands especially during

417 winter, the dry season (Mucina and Rutherford, 2006). The Limpopo paleoenvironmental dataset

418 shows an increase in aridity after 1 Ma that may support the evidence from sediments, fauna and

419 phytoliths (Caley et al., 2018).

420   This C_4 grassland environment persisted in the LOC, as evidenced by the low-energy water

421 deposition of clay and fine gravel beds with multiple bone scatters of Cornelian age, and by root

422 casts indicative of ancient land surfaces. However, the sharp boundary with the MYC might

423 represent a relatively brief period of high-energy water erosion that removed the original land

424 surface. A similar process likely stripped the latest land surface of the LOC and subsequently

425 deposited the OCG. As mentioned for the meandering river, the deposition of coarse gravel might

426 be a result of knickpoint exposure further upstream, which caused an increase in slope, a decrease

427 in sinuosity, and thus a more rapid flow able to transport coarser clasts (Tooth et al., 2004). The

428 presence of dolerite pebbles in the OCG and not in sedimentary units above and below seems to

429 support this interpretation, as these components would derive from the erosion of exposed dolerite.

430 In addition, the regional trend towards increased aridity after 1 Ma (Caley et al., 2018) seems to

431 exclude higher flow regime from the source as a possible cause for increased water energy and

432 coarser sediment supply. The absence of faunal material in the OCG and the lack of data from other

433 proxies (e.g. phytoliths, pollen) hinder a proper reconstruction of the paleoenvironment at this stage.

434 Nevertheless, the occurrence of younger Acheulean artifacts towards the top of the OCG (Brink et

435 al., 2012), perhaps transported by water, indicates that humans were present in the area.

436 Additionally, the persistence of C_4 grasslands in the Highveld from the Cornelian through to the

437 Florisian LMA as shown by faunal evidence (e.g. Brink, 1987, 1988; Lacruz et al., 2002; Brink,

438 2004; Codron et al., 2008; Brink et al., 2012; Brink et al., 2015; Brink, 2016), suggests that this

439 kind of environment existed also at the time of deposition of the OCG. This is further confirmed by

440 the fine alluvium altered by pedogenesis that makes up the BTS, the last layer deposited by the

441 paleo-Schoonspruit during a meandering stage similar to previous ones, before the beginning of its

442 current incising phase in the study area.

443 **5 Conclusions**

444 Cornelia-Uitzoek is the type locality of the Cornelian LMA (~1.1-0.6 Ma) and has produced a large

445 faunal assemblage dated to ~1.0 Ma that is the result of bone accumulation by hyenas. In addition,

446 the occurrence of a human tooth and several Acheulean artifacts indicates that hominins occupied

447 the area around the site. This important paleoecological occurrence offered the opportunity to study

448 in depth the environments in which humans lived, in a region that features an extremely limited

449 number of human fossils. Using a microgeoarchaeological approach based on FTIR spectroscopy

450 and micromorphology of sediments, we were able to identify mineral phases and microscopic

451 sedimentary structures typical of deposition by low- and high-energy water, and thus we could

452 determine the formation and post-depositional processes of the entire stratigraphic sequence,

453 including the bone bed that yielded the faunal and lithic assemblages. What emerged is an alluvial

454 environment dominated by local geology, which determined the amount and type of sediment

455 supply. Phases of low-energy water deposition in a meandering river system were conducive to the

456 formation of oxbows and backswamps that supported populations of large- to small-sized ungulates,

457 as well as carnivores and humans. Instead, high-energy water led to erosional hiatuses in the

458 stratigraphy and to the deposition of coarse material, bearing little or no faunal/lithic evidence.

459 Increasing aridity as seen at a regional level in southeastern Africa and locally based on the

460 presence of post-depositional shrink/swell and redoximorphic features, faunal assemblages and

stable isotopes datasets, points to C_4 grasslands as the dominant biome, which later expanded in the Florisian LMA. Faunal and sedimentary evidence highlight the role of the central interior of South Africa as favorable habitat for the evolution of early hominins, and the importance of addressing site-formation and post-depositional processes by looking also at the microscopic record.

Acknowledgements

References

Bender, P.A., Brink, J.S., 1992. A preliminary report on new large mammal fossil finds from the Cornelia-Uitzoek site, South African Journal of Science 88, 512-515.
Brink, J.S., 1987. The archaeozoology of Florisbad, Orange Free State, Memoirs van die Nasionale Museum, Bloemfontein 24, 1-151.
Brink, J.S., 1988. The taphonomy and palaeoecology of the Florisbad spring fauna, Palaeoecology of Africa and the Surrounding Islands 19, 169-179.
Brink, J.S., Rossouw, L., 2000. New trial excavations at the Cornelia-Uitzoek type locality, Navorsinge van die Nasionale Museum Bloemfontein 16, 141-156.
Brink, J.S., Henderson, Z.L., 2001. A high-resolution Last Interglacial MSA horizon at Florisbad in the context of other open-air occurrences in the central interior of southern Africa: an interim statement, in: Conard, N.J. (Ed.), Settlement dynamics of the Middle Paleolithic and Middle Stone Age, Kerns Verlag, Tübingen, pp. 1-20.
Brink, J.S., 2004. The taphonomy of an Early/Middle Pleistocene hyaena burrow at Cornelia-Uitzoek, South Africa, Revue de Paléobiologie 23, 731-740.
Brink, J.S., Herries, A.I.R., Moggi-Cecchi, J., Gowlett, J.A.J., Bousman, C.B., Hancox, J.P., Grün, R., Eisenmann, V., Adams, J.W., Rossouw, L., 2012. First hominine remains from a ~1.0 million year old bone bed at Cornelia-Uitzoek, Free State Province, South Africa, Journal of Human Evolution 63, 527-535.

500   Brink, J.S., Bousman, C.B., Grün, R., 2015. A reconstruction of the skull of *Megalotragus priscus*
501   (Broom, 1909), based on a find from Erfkroon, Modder River, South Africa, with notes on
502   the chronology and biogeography of the species, Palaeoecology of Africa 33, 71-94.
503   Brink, J.S., 2016. Faunal evidence for a mid- and late Quaternary environmental change in southern
504   Africa, in: Knight, J., Grab, S.W. (Eds.), Quaternary environmental change in southern
505   Africa: physical and human dimensions, Cambridge University Press, Cambridge.
506   Butzer, K.W., 1974. Geology of the Cornelia Beds, Memoirs van die Nasionale Museum,
507   Bloemfontein 9, 7-32.
508   Caley, T., Extier, T., Collins, J.A., Schefuß, E., Dupont, L., Malaizé, B., Rossignol, L., Souron, A.,
509   McClymont, E.L., Jimenez-Espejo, F.J., García-Comas, C., Eynaud, F., Martinez, P., Roche,
510   D.M., Jorry, S.J., Charlier, K., Wary, M., Gourves, P.-Y., Billy, I., Giraudeau, J., 2018. A
511   two-million-year-long hydroclimatic context for hominin evolution in southeastern Africa,
512   Nature 560, 76-79.
513   Clark, J.D., 1974. The stone artefacts from Cornelia, O.F.S., South Africa, Memoirs van die
514   Nasionale Museum, Bloemfontein 9, 33-62.
515   Codron, D., Brink, J.S., Rossouw, L., Clauss, M., 2008. The evolution of ecological specialization
516   in southern African ungulates: competition- or physical environmental turnover?, Oikos
517   117, 344-353.
518   Cooke, H.B.S., 1974. The fossil mammals of Cornelia, O.F.S., South Africa, Memoirs van die
519   Nasionale Museum, Bloemfontein 9, 63-84.
520   Courty, M.A., Goldberg, P., Macphail, R.I., 1989. Soils and Micromorphology in Archaeology,
521   Cambridge University Press, Cambridge.
522   Delvigne, J.E., 1998. Atlas of micromorphology of mineral alteration and weathering,
523   Mineralogical Association of Canada, Ottawa.
524   deMenocal, P.B., 2004. African climate change and faunal evolution during the Pliocene-
525   Pleistocene, Earth and Planetary Science Letters 220, 3-24.
526   Eriksson, P.G., Altermann, W., 1998. An overview of the geology of the Transvaal Supergroup
527   dolomites (South Africa), Environmental Geology 36, 179-188.
528   Farmer, V.C., 1974. The Infrared Spectra of Minerals, Mineralogical Society, London.
529   Flügel, E., 2004. Microfacies of carbonate rocks: Analysis, interpretation and application, Springer,
530   Berlin.
531   Geiger, S.B., Weiner, S., 1993. Fluoridated carbonatoapatite in the intermediate layer between glass
532   ionomer and dentin, Dental Materials 9, 33-36.
533   Goldberg, P., Macphail, R.I., 2006. Practical and Theoretical Geoarchaeology, Blackwell
534   Publishing, Malden, MA.
535   Goldberg, P., Berna, F., 2010. Micromorphology and context, Quaternary International 214, 56-62.
536   Goldberg, P., Aldeias, V., 2018. Why does (archaeological) micromorphology have such little
537   traction in (geo)archaeology?, Archaeological and Anthropological Sciences 10, 269-278.
538   Helgren, D.M., 1978. Acheulian settlement along the lower Vaal River, South Africa, Journal of
539   Archaeological Science 5, 39-60.
540   Hendey, Q.B., 1974. The Late Cenozoic Carnivora of the South-Western Cape Province, Annals of
541   the South African Museum 63, 1-369.
542   Karkanas, P., Goldberg, P., 2019. Reconstructing Archaeological Sites: Understanding the
543   Geoarchaeological Matrix, Wiley Blackwell.
544   Kooistra, M.J., Pulleman, M.M., 2010. Features Related to Faunal Activity, in: Stoops, G.,
545   Marcelino, V., Mees, F. (Eds.), Interpretation of micromorphological features of soils and
546   regoliths, Elsevier, Amsterdam, pp. 397-418.
547   Kovda, I., Mermut, A.R., 2010. Vertic Features, in: Stoops, G., Marcelino, V., Mees, F. (Eds.),
548   Interpretation of micromorphological features of soil and regoliths, Elsevier, Amsterdam,
549   pp. 109-127.

550 Kuman, K., Inbar, M., Clarke, R.J., 1999. Palaeoenvironments and Cultural Sequence of the
551   Florisbad Middle Stone Age Hominid Site, South Africa, Journal of Archaeological Science
552   26, 1409-1425.
553 Kuman, K., 2016. Development of the archaeological record in southern Africa during the Earlier
554   Stone Age, in: Knight, J., Grab, S. (Eds.), Quaternary Environmental Change in Southern
555   Africa: Physical and Human Dimensions, Cambridge University Press, Cambridge, pp. 349-
556   370.
557 Kuman, K., Gibbon, R.J., 2018. The Rietputs 15 site and Early Acheulean in South Africa,
558   Quaternary International 480, 4-15.
559 Lacruz, R., Brink, J.S., Hancox, P.J., Skinner, A.R., Herries, A.I.R., Schmid, P., Berger, L.R., 2002.
560   Palaeontology and geological context of a Middle Pleistocene faunal assemblage from the
561   Gladysvale Cave, South Africa, Palaeontologia Africana 38, 99-114.
562 LeGeros, R.Z., 1991. Calcium Phosphates in Oral Biology and Medicine, Karger, Basel,
563   Switzerland.
564 Li, H., Kuman, K., Lotter, M.G., Leader, G.M., Gibbon, R.J., 2017. The Victoria West: earliest
565   prepared core technology in the Acheulean at Canteen Kopje and implications for the
566   cognitive evolution of early hominids, Royal Society Open Science 4, 170288.
567 Lindbo, D.L., Stolt, M.H., Vepraskas, M.J., 2010. Redoximorphic Features, in: Stoops, G.,
568   Marcelino, V., Mees, F. (Eds.), Interpretation of micromorphological features of soils and
569   regoliths, Elsevier, Amsterdam, pp. 129-147.
570 Loock, J.C., Grobler, N.J., 1988. The regional geology of Florisbad, Navorsinge van die Nasionale
571   Museum Bloemfontein 5, 489-497.
572 Lyons, R., Tooth, S., Duller, G.A.T., 2014. Late Quaternary climatic changes revealed by
573   luminescence dating, mineral magnetism and diffuse reflectance spectroscopy of river
574   terrace palaeosols: a new form of geoproxy data for the southern African interior,
575   Quaternary Science Reviews 95, 43-59.
576 Macphail, R.I., Goldberg, P., 2017. Applied Soils and Micromorphology in Archaeology,
577   Cambridge University Press, Cambridge.
578 Mason, R.J., 1961. The Acheulean Culture in South Africa, South African Archaeological Bulletin
579   16, 107-110.
580 Mucina, L., Rutherford, M.C., 2006. The Vegetation of South Africa, Lesotho and Swaziland,
581   South African National Biodiversity Institute, Pretoria.
582 Newesely, H., 1989. Fossil bone apatite, Applied Geochemistry 4, 233-245.
583 Piga, G., Santos-Cubedo, A., Brunetti, A., Piccinini, M., Malgosa, A., Napolitano, E., Enzo, S.,
584   2011. A Multi-technique approach by XRD, XRF, FT-IR to characterize the diagenesis of
585   dinosaur bones from Spain, Palaeogeography, Palaeoclimatology, Palaeoecology 310, 92-
586   107.
587 Scott, L., Neumann, F.H., 2018. Pollen-interpreted palaeoenvironments associated with the Middle
588   and Late Pleistocene peopling of Southern Africa, Quaternary International 495, 169-184.
589 Soil Classification Working Group, 1991. Soil Classification - a Taxonomic System for South
590   Africa, Department of Agricultural Development, Pretoria.
591 Stoops, G., 2003. Guidelines for Analysis and Description of Soil and Regolith Thin Sections, Soil
592   Science Society of America, Madison, WI.
593 Stoops, G., Marcelino, V., Mees, F., 2010. Interpretation of Micromorphological Features of Soils
594   and Regoliths, Elsevier, Amsterdam.
595 Toffolo, M., Berna, F., 2008. Analisi micromorfologica, FTIR e XRD, in: Gelichi, S., Piuzzi, F.,
596   Cianciosi, A. (Eds.), "Sachuidic presso Forni Superiore". Ricerche archeologiche in un
597   castello della Carnia, Edizioni all'Insegna del Giglio, Florence, pp. 50-55.
598 Toffolo, M.B., Brink, J.S., Berna, F., 2015. Bone diagenesis at the Florisbad spring site, Free State
599   Province (South Africa): Implications for the taphonomy of the Middle and Late Pleistocene
600   faunal assemblages, Journal of Archaeological Science: Reports 4, 152-163.

601   Toffolo, M.B., Brink, J.S., van Huyssteen, C., Berna, F., 2017. A microstratigraphic reevaluation of
602   the Florisbad spring site, Free State Province, South Africa: Formation processes and
603   paleoenvironment, Geoarchaeology 32, 456-478.
604   Tooth, S., McCarthy, T.S., Brandt, D., Hancox, P.J., Morris, R., 2002. Geological controls on the
605   formation of alluvial meanders nd floodplain wetlands: the example of the Klip River,
606   eastern Free State, South Africa, Earth Surface Processes and Landforms 27, 797-815.
607   Tooth, S., Brandt, D., Hancox, P.J., McCarthy, T.S., 2004. Geological controls on alluvial river
608   behaviour: a comparative study of three rivers on the South African Highveld, Journal of
609   African Earth Sciences 38, 79-97.
610   van der Marel, H.W., Beutelspacher, H., 1976. Atlas of Infrared Spectroscopy of Clay Minerals and
611   their Admixtures, Elsevier Scientific Publishing Company, Amsterdam.
612   van Hoepen, E.C.N., 1930. Fossiele perde van Cornelia, O.V.S., Paleontologiese Navorsing van die
613   Nasionale Museum Bloemfontein 2, 1-24.
614   van Hoepen, E.C.N., 1932a. Voorlopige beskrywing van Vrystaatse soogdiere, Paleontologiese
615   Navorsing van die Nasionale Museum Bloemfontein 2, 63-65.
616   van Hoepen, E.C.N., 1932b. Die stamlyn van die sebras, Paleontologiese Navorsing van die
617   Nasionale Museum Bloemfontein 2, 25-37.
618   van Hoepen, E.C.N., 1947. A preliminary description of new Pleistocene mammals of South Africa,
619   Paleontologiese Navorsing van die Nasionale Museum Bloemfontein 7, 103-106.
620   Vingiani, S., Minieri, L., Livadie, C.A., Di Vito, M.A., Terribile, F., 2018. Pedological
621   investigation of an early Bronze Age site in southern Italy, Geoarchaeology 33, 193-217.
622   Weiner, S., 2010. Microarchaeology. Beyond the Visible Archaeological Record, Cambridge
623   University Press, New York.

624

625   **Captions**

626   **Figure 1.** Map of southern Africa showing the location of Cornelia-Uitzoek.

627   **Figure 2.** General view of Cornelia-Uitzoek, looking north.

628   **Figure 3.** View of the shale bedrock and basal Banded Gravel Bed, looking north. Note the deep

629   incision cut into bedrock by the river and the erosional boundary between sedimentary units.

630   **Figure 4.** View of the Banded Gravel Bed and overlying Mottled Yellow Clay, looking south

631   (scale: 20 cm). The trench cross-cuts the bone bed. Solid line marks the boundary between

632   sedimentary units; dashed line marks the limit of the bone bed; white blocks and square are

633   micromorphology samples discussed in the text. Note faunal material in the section (arrows).

634   **Figure 5.** View of the Mottled Yellow Clay and Laminated Orange Clay, looking north. The

635   boundary between sedimentary units roughly coincides with the foot of the donga. Note horizontal

636   laminations in the erosional profiles.

637   **Figure 6.** View of the Laminated Orange Clay, looking east. Squares mark micromorphology

638   blocks (trowel: 15 cm).

Figure 7. View of the Laminated Orange Clay and Orange Coarse Gravel, looking south (scale: 20 cm). Note the erosional boundary between sedimentary units and vertical root casts. Square marks a micromorphology block.

Figure 8. View of the Laminated Orange Clay, Orange Coarse Gravel, Dark Grey Clay and Black Turf Soil, looking south (trowel: 15 cm). Note the diffuse boundary between topsoil and Orange Coarse Gravel. Squares mark micromorphology blocks.

Figure 9. Representative FTIR spectra of sediments from Cornelia-Uitzoek.

Figure 10. Photomicrographs of representative thin sections from Cornelia-Uitzoek; all images in plane polarized light, except for D in crossed polarized light. A and B: MYC, fragmented clay crusts embedded within the MYC; C: MYC, rounded shale pellet from bone bed deposit; D: MYC, striated b-fabric (lighter orange stringers) indicative of shrink/swell processes; E and F: MYC, juxtaposed coatings of dark-green and yellow clay, bone bed deposit; G: MYC, Fe-Mn oxides aggregate nodules (arrows) superimposed on clay coatings (pale yellow sediment in void); H: MYC, Fe-Mn oxides coating and hypocoating (red-brown halos) around channel.

Figure 11. Photomicrographs of representative thin sections from Cornelia-Uitzoek; all images in plane polarized light, except for E in crossed polarized light. A: LOC, Fe-Mn oxides impregnative feature on groundmass (darker hue), note the marked boundary; B: LOC, coarse, dense infilling of red clay and silt from overlying layers, caused by a root channel; C: LOC, shale pellets bound by bridges of dark-green and yellow clay coatings; D: LOC, juxtaposed coatings of dark-green and yellow clay; E: OCG, dolerite fragment; F: OCG, orthic (left) and disorthic (right) typic nodules of Fe-Mn oxides; G: OCG, orthic concentric nodule of Fe-Mn oxides (arrow); H: BTS, ellipsoid excrements deposited by mites (brown rounded dots).

Figure 12. General view of the donga, looking north. Note the numerous vertical root casts that run through the Orange Coarse Gravel and Laminated Orange Clay. In the latter, cross-sections of the casts are visible from the surface (profile in the background).

Figure 13. Pebbles of shale and dolerite coated with Fe-Mn oxides that formed at the boundary between BTS and OCG. These components are a lag deposit produced by the erosion of BTS and OCG during donga advancement (scale: 20 cm).

Figure 14. View of the topsoil, looking east. Areas that lost plant cover due to donga advancement (arrows) appear dark grey in color due to the oxidation of organic matter in BTS. This deposit occurs in patches at the edge of the donga and was named Dark Grey Clay by Brink et al. (2012).

670   **Figure 15.** General view of the donga, looking east. Note channeling caused by water erosion

671   (arrows).

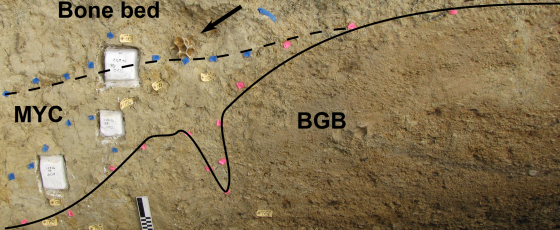**Bone bed**

Valley fill and donga

Schoonspruit

BGB

Ecca shale

Bone bed

MYC

BGB
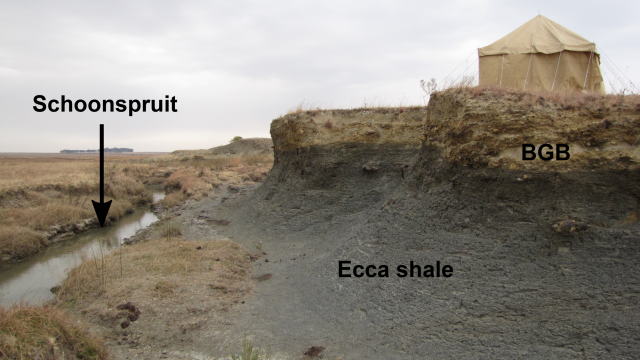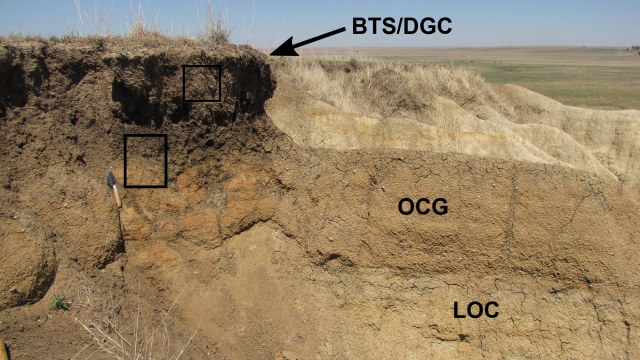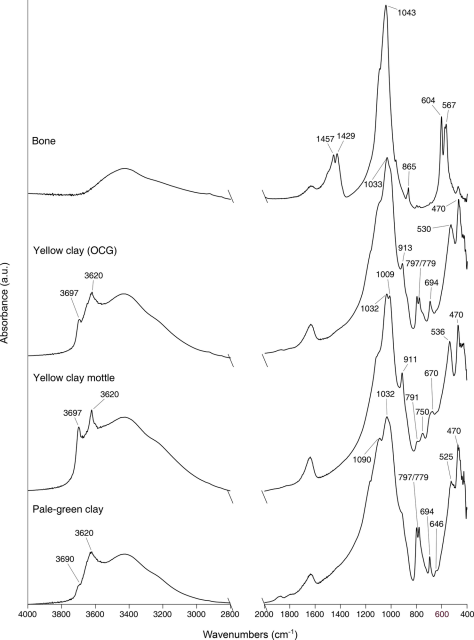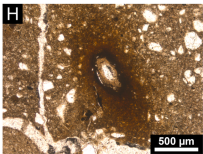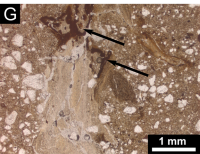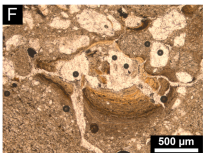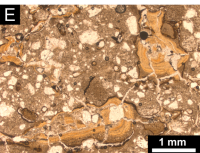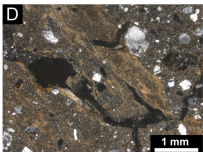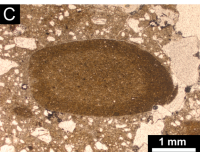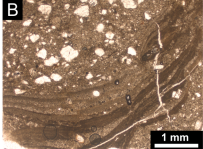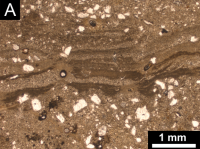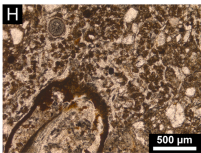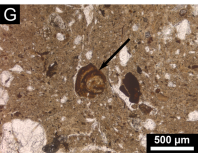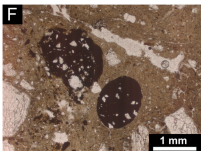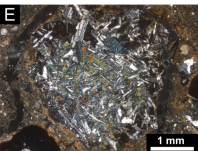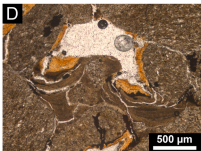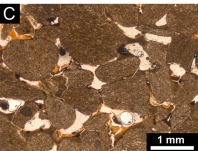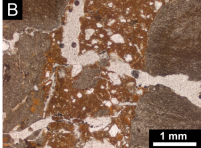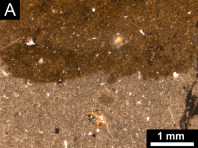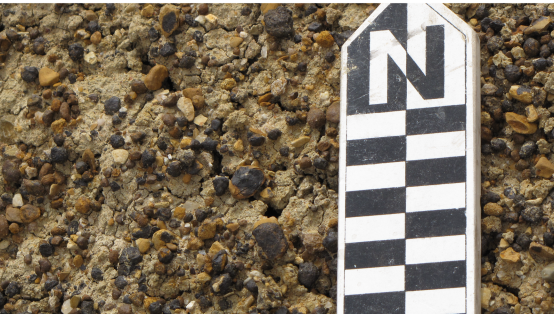
LOC

Table 1. Sedimentary units identified at Cornelia-Uitzoek from top to bottom, including data from Brink et al. (2012). Ages are based on paleomagnetism.

Unit	Description	Age (Ma)
Black Turf Soil (BTS)	Topsoil composed of dark brown clay, about 50 cm thick; it contains Middle Stone Age artifacts in places	<0.78
Dark Grey Clay (DGC)	Layer composed of dark grey clay, about 50 cm thick, contiguous to BTS; it contains younger Acheulean artifacts	<0.78
Orange Coarse Gravel (OCG)	Layer composed of gravel, up to 2 m thick at some locations	<0.78
Laminated Orange Clay (LOC)	Layer composed of alternating beds of clay and fine gravel, 2 m thick; it contains small clusters of bones	0.99-0.78
Mottled Yellow Clay (MYC)	Layer of massive pale-yellow to pale-green clay, 3 m thick; it contains a bone bed accumulated by hyenas and Acheulean artifacts	1.07-0.99
Banded Gravel Bed (BGB)	Layer of gravel characterized by normal graded bedding, 1 m thick	>1.07

Table 2. Microfacies types (MFT) identified at Cornelia-Uitzoek. The terminology follows Stoops (2003). MFTs as defined by Flügel (2004).

MFT name	Description	Formation process	Layer
Clay	**c/f related distribution:** close porphyric to open porphyric. **Structure and voids:** weakly to moderately separated angular blocky microstructure with planes and few channels. **Coarse fraction:** sub-angular, silt-sized quartz and feldspar grains (dominant); sub-rounded to sub-angular, medium sand- to very fine sand-sized quartz and feldspar grains (common); rounded, coarse sand- to very fine pebble-sized shale pellets (few). **Fine fraction:** pale-green clay with stipple speckled b-fabric, and in places monostriated, cross-striated, porostriated and granostriated b-fabric. **Pedofeatures:** dusty dark-green clay coatings on voids with striated b-fabric; dusty dark-green clay intercalations with striated b-fabric; limpid yellow clay laminated coatings on voids with striated b-fabric; limpid yellow clay dense infillings with striated b-fabric; moderately to strongly impregnated Fe-Mn oxide orthic aggregate nodules in groundmass, shale pellets and clay coatings/infillings; Fe-Mn oxide hypocoatings and quasicoatings on voids; dark-green clay crusts with striated b-fabric; red silty clay dense infillings with stipple speckled b-fabric; limpid red clay laminated coatings on voids with striated b-fabric.	Overbank deposit (meandering river), shrink/swell, fine and coarse illuviation	MYC, LOC
Fine gravel	**c/f related distribution:** chitonic to concave gefuric. **Structure and voids:** weakly separated granular microstructure to vughy microstructure, with compound packing voids, regular vughs and star-shaped vughs. **Coarse fraction:** rounded, coarse sand- to medium pebble-sized shale pellets (very dominant); sub-rounded, medium sand-sized quartz grains (very few). **Fine fraction:** pale-green clay with stipple speckled b-fabric, and in places granostriated b-fabric. **Pedofeatures:** dusty dark-green clay coatings on voids with striated b-fabric; limpid yellow clay laminated coatings on voids and shale pellets with striated b-fabric; limpid yellow clay dense infillings with striated b-fabric; moderately to strongly impregnated Fe-Mn oxide orthic aggregate nodules in groundmass, shale pellets and clay coatings/infillings; Fe-Mn oxide hypocoatings of voids.	Overbank deposit (meandering river), shrink/swell, fine illuviation	LOC
Coarse gravel	**c/f related distribution:** close porphyric to open porphyric. **Structure and voids:** weakly to moderately separated angular blocky microstructure with planes and few channels. **Coarse fraction:** sub-angular, silt-sized quartz and feldspar grains (frequent); sub-angular to sub-rounded, medium sand- to very fine sand-sized quartz and feldspar grains (frequent); rounded, coarse sand- to very coarse pebble-sized dolerite fragments (few); rounded, coarse sand- to pebble-sized shale pellets (few); elongated fragments of plant tissue (very few). **Fine fraction:** pale-brown clay with random striated, granostriated and porostriated b-fabric. **Pedofeatures:** strongly impregnated Fe-Mn oxide orthic and disorthic typic nodules; weakly impregnated Fe-Mn oxide orthic aggregate nodules on groundmass.	Channel/point bar deposit (meandering river), shrink/swell, eluviation	OCG
Topsoil	**c/f related distribution:** close porphyric. **Structure and voids:** massive microstructure with rare channels. **Coarse fraction:** sub-angular, silt-sized quartz and feldspar grains (dominant); sub-angular to sub-rounded, medium sand- to very fine sand-sized quartz and feldspar grains (common); elongated plant fibers (very few). **Fine fraction:** dark-brown clay with undifferentiated b-fabric; amorphous organic matter. **Pedofeatures:** strongly impregnated Fe-Mn oxide orthic and disorthic typic nodules; spherical and ellipsoid excrements.	Overbank deposit (meandering river), pedogenesis	BTS, DGC